ChemComm

COMMUNICATION

View Article Online
View Journal | View Issue

Check for updates

Cite this: *Chem. Commun.*, 2023, **59**, 6187

Received 19th March 2023,
Accepted 21st April 2023

DOI: 10.1039/d3cc01348k

rsc.li/chemcomm

From waste plastics to layered porous nitrogen-doped carbon materials with excellent HER performance†

Chao Juan, Bing Lan, Chuanchuan Zhao, Hualong Zhang, Dan Li* and
Fan Zhang *

Herein, layered porous nitrogen-doped carbon sheets (LPNCS) prepared from waste plastics are employed as an electrocatalytic carrier for the HER under alkaline conditions. The N-doped coral-like nanostructure with abundant meso- and macropores would shorten the proton diffusion pathway, reduce the mass transfer resistance and promote Ru dispersion. The prepared Ru/LPNCS shows an excellent performance with an overpotential of 15 mV at 10 mA cm^{-2}, even lower than that of most reported Ru-based catalysts and the commercial Pt/C catalyst (17 mV), which provides a potential application for converting waste plastics into highly efficient HER catalysts.

With the increasing serious energy and pollution crisis, people are vigorously developing sustainable energy.[1] Hydrogen, one of the cleanest and eco-friendly fuels with the largest energy density and zero-emission of carbonaceous species, is recognized as the best alternative to fossil fuels and a promising medium for storing energy from other sustainable resources such as solar, wind, and hydroelectric power.[2] Among the current hydrogen production methods, the hydrogen evolution reaction (HER), the half-reaction of water electrolysis, can convert intermittent renewable energy into hydrogen energy.[3] Noble metal catalysts are considered to be the most effective HER catalysts due to their high activity and stability.[4] To maximize their utilization, they are usually fixed to a supporting matrix to enhance dispersion and prevent aggregation during synthesis and reaction. Carbon-based materials are considered as excellent catalyst carriers due to the high conductivity of the graphite skeleton and the large specific surface area and porosity, which can not only facilitate the transfer of charge from the carbon support to the catalyst surface, but also improve the number of active sites and the transport rate of reactants and products.[5] Cheng *et al.*[6] synthesized highly dispersed and fine Ru nanoclusters on carbon black to improve the HER activity. Barman *et al.*[7] synthesized Ru nanocrystals on N-doped graphene, where the electron transfer of Ru to carbon leads to electron-deficient metal centers and thus improves HER activity. However, the synthesis of carbon materials is often complicated and requires the introduction of additional carbon sources. Thus, fabricating advanced carbon supports from sustainable carbon sources is significant for developing better HER catalysts.

On the other hand, the use of plastic provides excellent convenience to life, and the consumption of plastic products is sharply on the rise.[8] Unfortunately, in addition to their versatile properties, the stability of most plastic materials causes them to degrade extremely slowly in nature, posing a severe threat to the environment.[9] If this plastic waste problem cannot be well treated, the greenhouse gas emissions from plastics synthesis and incineration would reach 650 million tons of carbon dioxide equivalent by 2050, accounting for 15% of the global carbon budget.[10] In order to avoid the resulting environmental pollution and the waste of resources, chemical recycling and upcycling strategies have rapidly developed in recent years.[11–14] Plastics, which contain rich carbon elements, could be viewed as one of the best sources to prepare high-value carbon materials.[15–22] Luong *et al.*[20] converted mixed plastic waste into gram-scale flash graphene (FG) in one second by flash Joule heating (FJH), with a power cost of only 7.2 kJ g^{-1}. Liu *et al.*[21] efficiently carbonized waste polypropylene into carbon nanosheets for the active material in a working electrode with a specific capacitance of up to 349 F g^{-1}. Min *et al.*[22] carbonized mixed plastics to prepare three-dimensional hollow carbon spheres, which achieved 802 mA h g^{-1} after 500 cycles at 0.5 A g^{-1} in lithium-ion batteries. Although various applications of carbon materials from waste plastic are reported, their uses in the hydrogen evolution reaction are rarely covered.

Herein, we developed a facile method to transform waste plastics into layered porous nitrogen-doped carbon sheets

---

Key Laboratory of Green Chemistry and Technology, Ministry of Education, National Engineering Laboratory of Eco-Friendly Polymeric Materials (Sichuan), College of Chemistry, Sichuan University, Chengdu 610065, China.
E-mail: fanzhang@scu.edu.cn, danli@scu.edu.cn

† Electronic supplementary information (ESI) available. See DOI: https://doi.org/10.1039/d3cc01348k

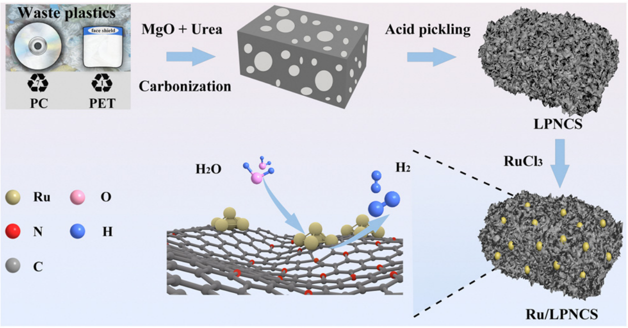

Scheme 1 Schematic of the synthesis route of LPNCS and Ru/LPNCS samples.

(LPNCS) as an electrocatalytic carrier, which were applied to produce green hydrogen in the HER under alkaline conditions. The prepared Ru/LPNCS showed an excellent performance in the HER with an overpotential of 15 mV at 10 mA cm^{-2}, even lower than that of most reported Ru-based catalysts and commercial Pt/C catalysts (17 mV). The layered porous structure of the carbon material obtained not only promotes contact with the electrolyte, but also changes Ru's electronic structure and its dispersion. We also used commercial plastics such as optical discs made of polycarbonate (PC) and polyethylene terephthalate (PET) masks to prepare carbon electrodes with an overpotential of 15 mV and 23 mV, respectively. This work suggests the potential applications of waste plastics as high-efficiency and low-cost HER electrocatalysts.

The overall synthesis route of the carbon materials from waste plastics is shown in Scheme 1. Firstly, waste plastics such as PC powders, optical discs, or PET masks are evenly mixed with magnesium oxide (MgO) in a mortar at room temperature. MgO has been selected as a template for preparing nanomaterials through plastic carbonization due to its low cost, adjustable morphology and easy removal.[23,24] In addition, by a control experiment, we speculate that MgO can also enhance the dispersion of waste plastic powder, which is crucial for forming a more uniform carbon material (Fig. S1, ESI†). Urea is chosen as the nitrogen source of N-doping and added in the first mixing step before calcination. Then, the mixed sample is placed in a tubular furnace and calcinated at 700 °C under a nitrogen atmosphere. After carbonization, the LPNCS is obtained after removing the MgO template by pickling. Finally, the Ru/LPNCS catalyst is prepared by conventional impregnation.

The carbonization process was analyzed by thermogravimetric analysis (TGA) (Fig. 1a and Fig. S2, ESI†). It showed a *ca.* 10% weight loss due to urea decomposition before 200 °C and a further 30% weight loss corresponding to the PC carbonation between 250 and 650 °C. No weight loss was observed after 700 °C. To investigate its surface area and pore structure, N_2 adsorption–desorption analysis was carried out. As shown in Fig. 1b and Table S1 (ESI†), the prepared sample exhibited a surface area of 666.5 m^2 g^{-1} and a pore volume of 0.355 cm^3 g^{-1}, and showed a type IV isotherm associated with a mesoporous structure. The Barrett–Joyner–Halenda (BJH) pore size distribution of the sample is shown in the inset of Fig. 1b. There were abundant micropores, mesopores and macropores in the sample, and the average pore size was calculated as 11.1 nm. The structure and morphology of the prepared carbon materials were further analyzed by scanning electron microscopy (SEM) and transmission electron microscopy (TEM). It shows a porous network like coral with interconnected carbon nanosheets (Fig. 1c). The TEM confirmed that the carbon nanosheets were like one or a few layers of graphene, wrinkled and overlapped to form coral-like nano-structures (Fig. 1d).

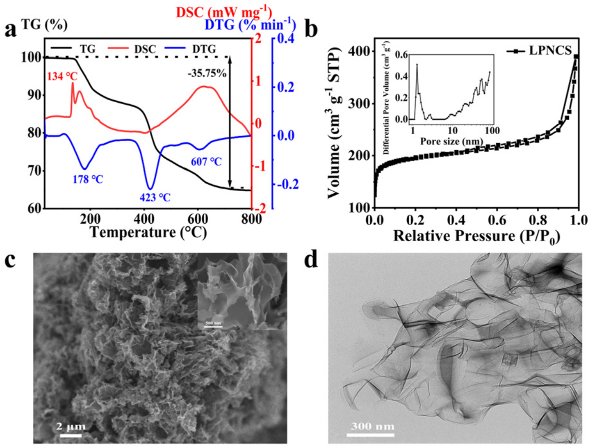

Fig. 1 (a) TG (black), DSC (red), and DTG (blue) curves of PC/MgO/Urea under a nitrogen atmosphere; (b) nitrogen adsorption/desorption isotherms and pore size distributions of LPNCS; (c) SEM and (d) TEM images of LPNCS.

After Ru loading, the morphology of Ru/LPNCS still maintained a layered porous structure, as shown in Fig. 2a, indicating that the loading and reduction process did not damage the coral structure of the carrier. High-angle annular dark-field scanning transmission electron microscopy (HAADF-STEM) images (Fig. 2b) showed that the nanoparticles were uniformly dispersed on the carbon skeleton with an average particle size of 3.2 nm. Energy dispersive X-ray spectroscopy (EDS) also showed that Ru was uniformly dispersed on LPNCS (Fig. S3, ESI† and Table S2, ESI†). Ru/LPNCS was tested by inductively coupled plasma-optical emission spectrometer (ICP-OES), and the Ru content was 2.13 wt%. In order to study the effect of different carbon materials on the dispersion of Ru, the same amount of Ru was loaded on activated carbon (Ru/AC) and undoped layered porous material (Ru/LPCS), respectively. The average particle sizes were increased to 12.4 nm for Ru/AC and 6.8 nm for Ru/LPCS (Fig. S4 and S5, ESI†), respectively. It can be seen that compared with Ru/AC and Ru/LPCS, Ru/LPNCS has higher metal dispersion and smaller Ru grain size, which may be due to N-doping and carbon sheet structure. This result was further confirmed by XRD (Fig. S6, ESI†) that Ru/LPNCS had a weaker and broader metal diffraction peak at 44°.[25] The surface area and pore structure of the catalysts are shown in Fig. 2c and Table S3 (ESI†). All of the catalysts had a type IV isothermal line, indicating a mesoporous structure. The BET surface areas of Ru/AC, Ru/LPCS and Ru/LPNCS were 1023.3, 868.5, and 736.3 m^2 g^{-1}, respectively. The BJH pore size distribution of the catalysts is

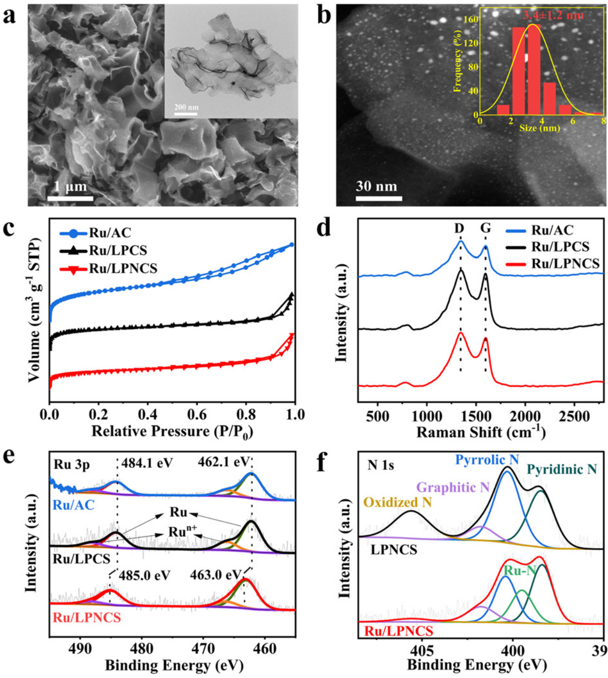

Fig. 2 (a) SEM and TEM images of Ru/LPNCS; (b) HAADF-STEM image and size distribution of Ru/LPNCS nanoparticles; (c) nitrogen adsorption/desorption isotherms and pore size distributions; (d) Raman spectra and (e) Ru 3p XPS spectra of the Ru/AC, Ru/LPCS, Ru/LPNCS; (f) N 1s XPS spectra of the LPNCS and Ru/LPNCS.

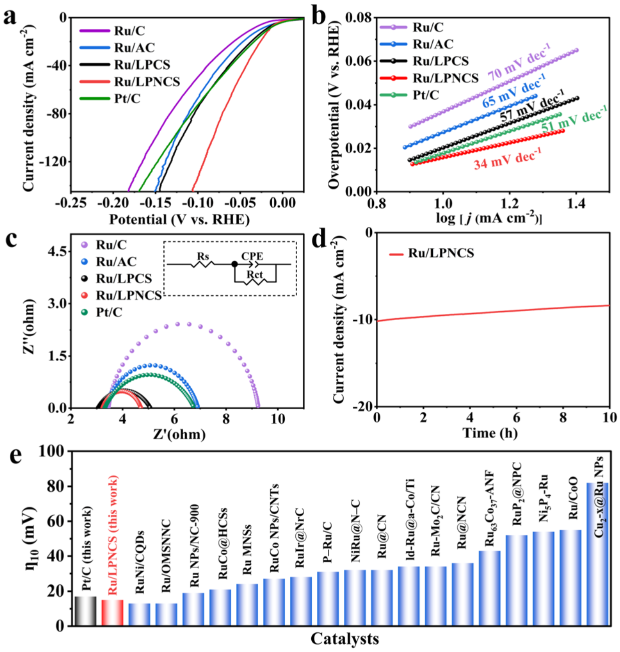

Fig. 3 (a) LSV curves, (b) Tafel plots and (c) Nyquist plots of commercial 5 wt% Ru/C, Ru/AC, Ru/LPCS, Ru/LPNCS and 20 wt% Pt/C in 1.0 M KOH; (d) *i*–*t* curve for Ru/LPNCS; (e) the comparison of the overpotentials for Ru/LPNCS with other recently reported HER electrocatalysts at 10 mA cm^{-2} in 1 M KOH.

shown in Fig. S7 (ESI†). There were abundant micropores and mesopores in all catalysts. In particular, Ru/LPCS and Ru/LPNCS had more macropores larger than 50 nm. Raman spectra of different catalysts (Fig. 2d) showed that the I_G/I_D ratios of Ru/LPNCS and Ru/LPCS were higher than in Ru/AC, indicating that the degree of graphitization was higher than in Ru/AC.

X-ray photoelectron spectroscopy (XPS) results are displayed in Fig. 2e and f, Fig. S8, and Table S4 (ESI†). The Ru 3p XPS revealed that the peaks at 462.1 and 484.1 eV for both Ru/AC and Ru/LPCS corresponded to metallic Ru species. The remaining two peaks at 466.0 and 488.0 eV correspond to Ru^{n+} species.[26] The peak for metallic Ru in Ru/LPNCS shifted 0.9 eV toward higher binding energy compared to Ru/AC and Ru/LPCS due to N doping. The N 1s spectrum of LPNCS could be deconvoluted into four individual types of N species, which belonged to pyridinic N (398.4 eV), pyrrolic N (400.4 eV), graphitic N (401.7 eV) and oxidized N (405.8 eV), respectively.[27] Importantly, after loading Ru, the content of pyrrole N was reduced due to the presence of Ru–N (19.64%). The XPS results indicate the transfer of electrons in the Ru nanoparticles to the interfacial Ru–N, confirming the presence of a strong electronic coupling effect on the surface.[25,27,28]

The HER electrocatalytic activity of the catalysts was measured in 1.0 M KOH by a typical three-electrode system. The activity of Ru/LPNCS was compared with pure LPNCS and other Ru catalysts by linear sweep voltammetry (LSV) curves (Fig. 3a and Fig. S9, ESI†). The overpotential at 10 mA cm^{-2} (η_{10}) of Ru/LPNCS was only 15 mV, which was significantly lower than that of Ru/LPCS (21 mV), Ru/AC (27 mV) and commercial 5 wt% Ru/C (37 mV). Notably, Ru/LPNCS even showed lower overpotential than 20 wt% Pt/C (17 mV). Ru/LPNCS prepared by optical discs (PC) and masks (PET) from real plastic carbon sources also showed excellent HER performance. When Ru/LPNCS-optical discs and Ru/LPNCS-mask were used as cathode catalysts (Fig. S10 and Table S5, ESI†), the η_{10} values were only 15 mV and 23 mV, respectively. Mass activity (MA) is an important component in evaluating precious metal catalysts' economic benefits.[27] As shown in Fig. S11 (ESI†), Ru/LPNCS had the highest activity (MA_{15mV} = 0.47 A mg^{-1}), which was 10 times higher than that of Pt/C (MA_{15mV} = 0.044 A mg^{-1}), and it had good economic value. The corresponding Tafel slopes of the three catalysts calculated from LSV curves are summarized in Fig. 3b. The Tafel slope of Ru/LPNCS was 34 mV dec^{-1}, less than the slope of commercial Pt/C (51 mV dec^{-1}). The results showed that the HER pathway for Ru/LPNCS was controlled by H* desorption through a typical Volmer–Tafel mechanism and had good reaction kinetics.[29] This may be due to the abundant meso- and macro-pores, which would shorten the proton diffusion pathway and reduce the mass transfer resistance.[30] Meanwhile, the higher degree of graphitization and the strong interaction between Ru nanoparticles and LPNCS also promotes electron transfer. This was further confirmed by the Nyquist diagram results (Fig. 3c), which showed that Ru/LPNCS had the smallest charge transfer resistance, so the electron/proton transfer rate was the fastest.[31] The double-layer capacitance (C_{dl}) was obtained by cyclic voltammograms (Fig. S12, ESI†). Ru/LPNCS had the highest C_{dl}, superior to Ru/AC and Ru/

LPCS. Since electrochemical surface area (ECSA) was proportional to C_{dl}, Ru/LPNCS had the largest ECSA value. It indicated a larger number of exposed active sites on Ru/LPNCS,[27,32] consistent with the higher Ru dispersion by TEM and XRD results. The catalyst stability was evaluated by the *i*–*t* curve (Fig. 3d), indicating that Ru/LPNCS had good durability. Interestingly, Ru/LPNCS (Fig. 3e and Table S6, ESI†) showed excellent HER electrocatalytic activity compared with catalysts reported in the previous literature. The above results show that the carbon material from waste plastics is an excellent carrier in the electrocatalytic reaction.

In summary, we have employed a simple method to transform waste plastics into coral-like layered porous nitrogen-doped carbon materials. Due to its higher degree of graphitization and abundant meso- and macro-pores, after Ru loading, the prepared Ru/LPNCS had an excellent HER performance, with the overpotential of only 15 mV at 10 mA cm^{-2}. It provides a viable path to dispose of waste plastics into functional carbon materials for electrocatalytic applications.

This paper was supported by the National Key Research and Development Program of China (No. 2021YFA1501700), the National Natural Science Foundation of China (No. 22272114), the Funding for Hundred Talent Program of Sichuan University (20822041E4079) and Open Project Funding of School of New Energy and Material of Southwest Petroleum University (NYTZGXCLSWPU202201). We thank Prof Hai-rong Yue and Shu-nan Yu from the School of Chemical Engineering of Sichuan University as well as Feng Yang and Jing Li from the College of Chemistry at Sichuan University for TEM testing.

Conflicts of interest

There are no conflicts to declare.

Notes and references

1 L. W. Xiong, Y. F. Qiu, X. Peng, Z. T. Liu and P. K. Chu, *Nano Energy*, 2022, **104**, 107882.
2 M. Amin, H. H. Shah, A. G. Fareed, W. U. Khan, E. Chung, A. Zia, Z. U. R. Farooqi and C. Lee, *Int. J. Hydrogen Energy*, 2022, **47**, 33112–33134.
3 I. Dincer, N. Javani and K. Karayel, *Sustainable Cities Soc.*, 2022, **87**, 104154.
4 J. Su, Y. Yang, G. Xia, J. Chen, P. Jiang and Q. Chen, *Nat. Commun.*, 2017, **8**, 14969.
5 Y. X. Li, X. F. Lu, S. B. Xi, D. Y. Luan, X. Wang and X. W. Lou, *Angew. Chem., Int. Ed.*, 2022, **61**, e202201491.
6 X. Cheng, H. Wang, M. Ming, W. X. Luo, Y. Wang, Y. C. Yang, Y. Zhang, D. J. Gao, J. Bi and G. Y. Fan, *ACS Sustainable Chem. Eng.*, 2018, **6**, 11487–11492.
7 B. K. Barman, D. Das and K. K. Nanda, *Sustainable Energy Fuels*, 2017, **1**, 1028–1033.
8 X. C. Jiao, K. Zheng, Z. X. Hu, S. Zhu, Y. F. Sun and Y. Xie, *Adv. Mater.*, 2021, **33**, 2005192.
9 L. Filiciotto and G. Rothenberg, *ChemSusChem*, 2021, **14**, 56–72.
10 J. Zheng and S. Suh, *Nat. Clim. Change*, 2019, **9**, 374–378.
11 F. Zhang, F. Wang, X. Y. Wei, Y. Yang, S. M. Xu, D. H. Deng and Y. Z. Wang, *J. Energy Chem.*, 2022, **69**, 369–388.
12 Z. W. Dong, W. J. Chen, K. Q. Xu, Y. Liu, J. Wu and F. Zhang, *ACS Catal.*, 2022, **12**, 14882–14901.
13 A. Rahimi and J. M. García, *Nat. Rev. Chem.*, 2017, **1**, 0046.
14 G. W. Coates and Y. D. Y. L. Getzler, *Nat. Rev. Mater.*, 2020, **5**, 501–516.
15 Z. W. Jiang, R. J. Song, W. G. Bi, J. Lu and T. Tang, *Carbon*, 2007, **45**, 449–458.
16 X. Jie, W. Li, D. Slocombe, Y. Gao, I. Banerjee, S. Gonzalez-Cortes, B. Yao, H. AlMegren, S. Alshihri, J. Dilworth, J. Thomas, T. Xiao and P. Edwards, *Nat. Catal.*, 2020, **3**, 902–912.
17 T. Tang, X. C. Chen, X. Y. Meng, H. Chen and Y. P. Ding, *Angew. Chem., Int. Ed.*, 2005, **44**, 1517–1520.
18 W. A. Algozeeb, P. E. Savas, D. X. Luong, W. Y. Chen, C. Kittrell, M. Bhat, R. Shahsavari and J. M. Tour, *ACS Nano*, 2020, **14**, 15595–15604.
19 W. A. Algozeeb, P. E. Savas, Z. Yuan, Z. Wang, C. Kittrell, J. N. Hall, W. Y. Chen, P. Bollini and J. M. Tour, *ACS Nano*, 2022, **16**, 7284–7290.
20 D. X. Luong, K. V. Bets, W. A. Algozeeb, M. G. Stanford, C. Kittrell, W. Chen, R. V. Salvatierra, M. Ren, E. A. McHugh, P. A. Advincula, Z. Wang, M. Bhatt, H. Guo, V. Mancevski, R. Shahsavari, B. I. Yakobson and J. M. Tour, *Nature*, 2020, **577**, 647–651.
21 X. G. Liu, C. D. Ma, Y. L. Wen, X. C. Chen, X. Zhao, T. Tang, R. Holze and E. Mijowska, *Carbon*, 2021, **171**, 819–828.
22 J. Min, X. Wen, T. Tang, X. Chen, K. Huo, J. Gong, J. Azadmanjiri, C. He and E. Mijowska, *Chem. Commun.*, 2020, **56**, 9142–9145.
23 J. Min, S. Zhang, J. Li, R. Klingeler, X. Wen, X. Chen, X. Zhao, T. Tang and E. Mijowska, *Waste Manage.*, 2019, **85**, 333–340.
24 Y. L. Wen, J. Liu, J. F. Song, J. Gong, H. Chen and T. Tang, *RSC Adv.*, 2015, **5**, 105047–105056.
25 Y. L. Wu, X. F. Li, Y. S. Wei, Z. M. Fu, W. B. Wei, X. T. Wu, Q. L. Zhu and Q. Xu, *Adv. Mater.*, 2021, **33**, 2006965.
26 H. Li, M. T. Zhang, L. C. Yi, Y. J. Liu, K. Chen, P. Shao and Z. H. Wen, *Appl. Catal., B*, 2021, **280**, 119412.
27 H. X. Yao, X. K. Wang, K. Li, C. Li, C. H. Zhang, J. Zhou, Z. W. Cao, H. L. Wang, M. Gu, M. H. Huang and H. Q. Jiang, *Appl. Catal., B*, 2022, **312**, 121378.
28 Q. Hu, G. Li, X. Huang, Z. Wang, H. Yang, Q. Zhang, J. Liu and C. He, *J. Mater. Chem. A*, 2019, **7**, 19531–19538.
29 E. H. Ma, T. Shen, D. F. Ying, W. Liu, X. Zhao, L. N. Zhang and D. L. Wang, *ACS Sustainable Chem. Eng.*, 2022, **10**, 15530–15537.
30 S. Q. Chen, S. Y. Fang, A. I. Lim, J. M. Bao and Y. H. Hu, *Chemosphere*, 2023, **322**, 138174.
31 J. Peng, Y. Chen, K. Wang, Z. Tang and S. Chen, *Int. J. Hydrogen Energy*, 2020, **45**, 18840–18849.
32 S. R. Wang, M. M. Wang, Z. Liu, S. J. Liu, Y. J. Chen, M. Li, H. Zhang, Q. K. Wu, J. H. Guo, X. Q. Feng, Z. Chen and Y. Pan, *ACS Appl. Mater. Interfaces*, 2022, **14**, 15250–15258.